Estimation of Zero-Field Activation Energy for Traps in Fe-and C-Doped GaN-Based HEMTs

P. Vigneshwara Raja, Vaidehi Vijay Painter, Emmanuel Dupouy, Raphaël Sommet, Jean-Christophe Nallatamby

Estimation of Zero-field Activation Energy for Traps in Fe- and C-doped GaN-based HEMTs

P. Vigneshwara Raja, Vaidehi Vijay Painter, Emmanuel Dupouy, Raphael Sommet, and Jean-Christophe Nallatamby

***Abstract*—Carrier emission rate accelerates from a trap with the increase in drain voltage due to the self-heating (SH) and Poole–Frenkel (PF) emission effects; thus the conventional Arrhenius analysis underestimates the trap activation energy. For this purpose, this work estimates the zero-field (actual) activation energy of a trap in InAlN/GaN and AlN/GaN HEMTs by including SH and PF effects in the emission rate equation. The HEMT thermal resistance (R_{TH}) is computed from the TCAD simulation results. Subsequently, the SH-induced increase in the channel temperature (ΔT) is incorporated in the Arrhenius plot, constructed from drain current transient (DCT) and output-admittance (Y_{22}) parameters. The apparent trap activation energy (E_{ap}) is calculated from the measured DCT and Y_{22} at different drain voltages, and the respective electric field (F) at each bias condition is extracted from the simulation. Finally, zero-field activation energy (E_0) is estimated from the E_{ap} vs. $(F)^{0.5}$ plot intercept. E_0 for the well-known Fe-related buffer trap is identified at E_C – 0.7 eV in the InAlN/GaN HEMT. Similarly, E_0 at E_C – 0.51 eV is found for the trap in the C-doped AlN/GaN HEMT.**

***Index Terms*—Drain current transient, GaN HEMT, output admittance, trap energy, self-heating, Poole-Frenkel.**

I. Introduction

DRAIN current transient (DCT) [1]-[7] and low-frequency (LF) output-admittance (Y_{22}) spectroscopy [8]-[13] are the widely used methods to identify the electrically active defects (traps) in the GaN-based high-electron mobility transistors (HEMTs). The DCT and Y_{22} measurements were conducted at numerous temperatures to construct an Arrhenius plot for a trap, by extracting the emission time constant at each temperature. It is known that the HEMT channel temperature rises with the augmentation in the drain voltage (V_{DS}) due to the self-heating (SH) effect. As a result, the carrier emission rate speeds up from a trap level due to the increased channel temperature [2], [12]. Suppose the Arrhenius analysis is made assuming that the channel temperature is the same as the base temperature of the thermal chuck/sample; in that case, the activation energy of the trap will be underestimated. Hence, the SH-induced increase in the channel temperature must be

accounted in the emission rate equation to eliminate the SH effect on the activation energy (E_a) calculation, as based on the work of Chini *et al.* [2]. Moreover, as the V_{DS} upsurges, the emission rate enhances due to the field-assisted carrier emission process (Poole-Frenkel (PF) emission) [8], [12], [14]. So, the PF emission-induced changes in the apparent E_a should be quantitatively evaluated as a function of V_{DS}, to estimate the zero-field thermal activation energy (E_0, binding energy of an electron at a trap without an external electric field) for the trap [12]. As a general rule of thumb, conducting the DCT and Y_{22} experiments at lower V_{DS} is preferable to minimize the SH and PF effects on E_a computation.

The InAlN/GaN HEMTs are a viable alternative to the widespread AlGaN/GaN HEMT technology for RF and microwave applications, due to their superior properties such as lattice-matched heterointerface, thin InAlN barrier, high spontaneous polarization, and absence of inverse piezoelectric phenomenon [5], [15]. The AlN/GaN heterostructure has received considerable interest in recent years, as they offer high 2DEG density (~6×10^{13} cm^{-2}), ultra-thin AlN barrier layer (≤ 6 nm) with a wide bandgap of 6.2 eV, and high spontaneous polarization [16]. For these reasons, InAlN/GaN and AlN/GaN HEMT structures are selected for this study. The compensational iron (Fe) doping is employed in the buffer layer of InAlN/GaN HEMT, while the GaN buffer region of AlN/GaN HEMT is doped with carbon (C) impurities.

The trapping-induced deteriorations in the HEMT dynamic characteristics become severe for deeper trap energies. Since the conventional Arrhenius analysis does not incorporate the impacts of SH and PF, it undervalues E_a. In fact, the exact E_a value should be chosen to precisely model the trapping/detrapping dynamics; this shows the importance of estimating the zero-field (actual) trap activation energy (E_0). Cioni *et al.* [6] independently analyzed the SH and PF effects on the emission time constant of the Fe-related buffer trap at E_C - 0.52 eV in the AlGaN/GaN HEMTs. The authors observed that the emission rate is unaffected by the V_{DS}

P. Vigneshwara Raja and Vaidehi Vijay Painter are with Department of Electrical Engineering, Indian Institute of Technology Dharwad, Karnataka-580011, India (e-mail: vigneshwararaja@iitdh.ac.in).

Emmanuel Dupouy, Raphael Sommet, and Jean-Christophe Nallatamby are with the XLIM Laboratory, CNRS, UMR 7252, University of Limoges, F-19100 Brive, France (e-mail: jean-christophe.nallatamby@unilim.fr).

variations up to 40 V, with the supporting simulation inspections. We also noticed a peculiar observation in a few AlGaN/GaN HEMT devices, such that, the emission rate increased with the V_{DS} (noted from Y_{22} parameters), still the Arrhenius investigation yielded nearly the same E_a for the trap. However, the PF-induced reduction in E_a is clearly visible in most of our HEMTs [5], [11], (including the devices considered in this work) and in the literature [12], [14], [17], [18]. Note that, the field-assisted carrier emission was also observed from the non-coulombic traps existing in the semiconductors [19]. Kayis *et al.* [17] applied low-frequency noise (LFN) spectral characteristics (at four different V_{DS}) to determine E_0 (0.71 eV) for the trap in the AlGaN/GaN HEMT, through the linear extrapolation of E_a vs. $(V_{DS})^{0.5}$ plot. Recently, Oishi *et al.* [12] systematically investigated the SH and PF effects on the activation energy of the Fe-related trap in the AlGaN/GaN HEMTs, using LF Y_{22} measurements and TCAD simulations. After extracting R_{TH}, the authors computed E_0 (0.68 eV) for the Fe-related buffer trap from the E_{ap} vs. $(F)^{0.5}$ plot intercept. To extend their research, this work aims to estimate E_0 for the trap in two different HEMT structures and buffer doping technologies, such as Fe-doped InAlN/GaN HEMT and C-doped AlN/GaN HEMT. Furthermore, E_0 determined from the DCT is compared with that deduced from the Y_{22} spectroscopy for the Fe-doped InAlN/GaN HEMTs. The identified E_0 values (in two different HEMTs) are helpful in accurately modeling the trap activation energy in the HEMT simulations.

II. E_0 Estimation Procedure

Since the kinetic energy of electrons increases upwards (they tend to fall) in the energy band, the electron capture process is essentially decided by trap capture cross-section and free electrons in the conduction band (not by temperature). On the contrary, the electron emission process needs sufficient thermal energy to move from the lower energy state to the higher energy level. The thermal activation energy indicates the thermal energy required to release the electron from the trapped energy level to the conduction band by overcoming the potential barrier. The electron emission rate (e_n) associated with a trap level at E_C - E_T is given by [7]-[9]

$$e_n = \frac{\sigma_n v_{th} N_C}{g}\exp\left(-\frac{E_C - E_T}{kT}\right) = \frac{\sigma_n v_{th} N_C}{g}\exp\left(-\frac{E_{ap}}{kT}\right) \quad (1)$$

where σ_n is the trap capture cross-section, v_{th} is carrier thermal velocity, N_C is the effective density states in conduction band, g is the degeneracy factor, k is the Boltzmann constant, T is the temperature, and E_{ap} is the apparent activation energy. The Equation (1) is rearranged in such a way that is convenient for the Arrhenius plot analysis [4], [7]-[9]:

$$\ln(\tau_n T^2) = \frac{E_{ap}}{kT} - \ln\left(\frac{\sigma_n N_C v_{th}}{gT^2}\right) \quad (2)$$

where τ_n is the emission time constant of the trap (inverse of emission rate). Equation (2) does not account the SH and PF effects, as a result, the computed apparent activation energy E_{ap} is less than the actual E_0. At high V_{DS}, the HEMT active region temperature is greater than the base temperature (T_b) of the thermal chuck due to the SH effects. So, the absolute HEMT temperature (T) is equal to the sum of base temperature (T_b) and the SH-induced increase in the channel temperature (ΔT) [2], [12]

$$T = T_b + \Delta T = T_b + R_{TH} I_{DS} V_{DS} = T_b + R_{TH} P_D \quad (3)$$

where R_{TH} is the device thermal resistance, and the power dissipation (P_D) is the product of drain current (I_{DS}) and drain voltage (V_{DS}) [12], [21]. Once the R_{TH} and P_D values are known, ΔT is calculated at each bias condition based on the Equation (3). Accordingly, the Equation (2) is modified as follows:

$$\ln(\tau_n (T_b + \Delta T)^2) = \frac{E_{ap}}{k(T_b + \Delta T)} - \ln\left(\frac{\sigma_n N_C v_{th}}{g(T_b + \Delta T)^2}\right) \quad (4)$$

Due to the PF effect, the electric field lowers the potential barrier by a factor ΔE_{PF} and hence augments the electron emission rate from the trap [8], [6], [12], [14] (analogous to the Schottky barrier lowering in the metal/semiconductor junction [20]). Because of the field-assisted emission, the trapped electrons require quite lower thermal energy to transition from the defect energy state to the conduction band. Note that, the traditional Arrhenius analysis (without including SH and PF) provides only the apparent activation energy (E_{ap}). Indeed, E_0 is the thermal activation energy needed to stimulate the trap-assisted electron emission from the trap in the absence of an electric field (zero electric field). E_0 and E_{ap} are related to the electric field (F) by the following equation [12], [20]

$$E_{ap} = E_0 - \Delta E_{PF} = E_0 - \beta\sqrt{F} = E_0 - \sqrt{\frac{q}{\pi\varepsilon}F} \quad (5)$$

where q is the elementary charge, ε is the dielectric constant of GaN material, and β is the constant term combining the physical and material parameters. The apparent E_{ap} for the trap is calculated at different V_{DS} bias conditions. The corresponding electric field (F) at each bias is computed from the TCAD device simulations. Consequently, E_0 is estimated from the intercept of the E_{ap} vs. $F^{0.5}$ plot (linear interpolation method). The Arrhenius analysis equation comprising the SH and PF effects can be written as [6], [12]

$$\ln(\tau_n (T_b + \Delta T)^2) = \frac{E_0 - \Delta E_{PF}}{k(T_b + \Delta T)} - \ln\left(\frac{\sigma_n N_C v_{th}}{g(T_b + \Delta T)^2}\right) \quad (6)$$

III. Experiment and Simulation Details

A. HEMT Device Structure

The lattice-matched $In_{0.17}Al_{0.83}N$/GaN heterostructure was grown on a silicon carbide (SiC) substrate. The heteroepitaxial layer includes 2 μm thick Fe-doped GaN buffer layer, undoped GaN channel layer, 10 nm InAlN barrier layer, and thin (2 nm) GaN cap layer. The AlN/GaN HEMT epilayer structure consists of 2 nm GaN cap layer, 4 nm AlN barrier layer, undoped GaN channel layer, and 1 μm thick C-doped GaN buffer layer grown on the SiC substrate. The Fe-doped InAlN/GaN HEMT features an ultra-short gate length of 0.12μm, and a gate width of 50 μm with six fingers (6×50 μm size). The C-doped AlN/GaN HEMT has 0.12 μm gate length and 50 µm gate width with two fingers (size 2×50 µm). The silicon nitride (SiN) passivation was employed in both the HEMT structures to mitigate the surface trapping effects.

B. DCT and Y_{22} Characterization

The DCT and Y_{22} characterization procedure is described elsewhere [5], [7], [9]-[11], [22]. As a first step in the DCT, the traps in the HEMT were populated by synchronously pulsing the gate and drain voltages to a deep off-state bias condition (V_{GF}, V_{DF}) = (-6 V, 10 V) for 1 ms pulse width. At the end of the filling pulse, the HEMT was instantaneously switched to a semi-on bias point (V_{GM}, V_{DM}), and the emission transient due to the carrier detrapping was measured in the time range of 1 µs to 10 s. The DCT spectrum was acquired for various operating temperatures from 30 °C to 165 °C.

Before performing Y_{22} experiments, the standard short-open-load-through (SOLT) practice was employed to calibrate the vector network analyzer. The Y_{22} parameters were measured at a fixed on-state gate and drain bias voltages in the low-frequency range of 100 Hz to 10 MHz. The Y_{22} measurements were also conducted at several temperatures (30 °C to 165 °C) to compute the trap parameters from the Arrhenius plot [8]-[13].

The DCT and Y_{22} spectra were measured at five different drain voltage conditions (V_{DS} varying from 1 V to 9 V, with a fixed V_{GS}) to evaluate the field-assisted carrier emission (PF) effect on trap activation energy.

C. Simulation Setup

The main motive of the simulation is to compute the thermal resistance (R_{TH}) and the electric field (F) at each bias point [12]. The InAlN/GaN and AlN/GaN HEMT structures are created in the Sentaurus TCAD simulator [21]. The calibration procedure of the physics-based TCAD model and material parameters is explained in our earlier reports [5], [7], [9], [11], [16], [23]. The thermal contact (thermode) is placed at the bottom of the SiC substrate with a base temperature (T_b) of 303 K. The thermodynamic model [22] is enabled in the carrier transport model to include the SH effect on the HEMT characteristics. The thermode surface resistance for InAlN/GaN and AlN/GaN HEMTs was optimized to 10^{-4} cm^{2}K/V, 6×10^{-5} cm^{2}K/V, respectively. The surface donor states are placed at SiN/GaN cap interface with an energy level at E_C - 0.2 eV (trap density of 10^{13} cm^{-2} and $\sigma_n = \sigma_p = 10^{-15}$ cm^2). The surface donor energy was chosen based on the energy position (~0.2 eV) identified from the temperature-dependent Y_{21} frequency dispersion properties [11].

The Fe-related acceptor trap (F1) at E_C – 0.7 eV (with $\sigma_n = 5\times10^{-15}$ cm^2 and $\sigma_p = 10^{-18}$ cm^2) is included in the GaN buffer. A non-uniform doping profile (comprising two regions) is considered for the Fe-related trap (F1) to emulate the practical scenario [4], [24], [25]. In region-1, F1 concentration increases exponentially from the channel layer edge (3.5×10^{16} cm^{-3}) and reaches the maximum density (3×10^{18} cm^{-3}) at 0.5µm depth in the buffer layer. While, F1 distribution is constant in the region-2 with a large concentration of 3×10^{18} cm^{-3}. The trap (C1) at E_C – 0.45 eV ($\sigma_n = 2\times10^{-20}$ cm^2 and $\sigma_p = 10^{-20}$ cm^2) is considered in the buffer layer of AlN/GaN HEMT. The C1 concentration is varied step-like fashion (containing two regions) as per the literature reports [4], [26]; C1 concentrations for the region-1 and 2 are selected as 10^{17} cm^{-3} and 10^{18} cm^{-3}, respectively. These non-uniform doping profiles are advantageous in retaining the electron mobility and density in the channel due to the reduced defect-induced scattering and charge trapping effects (in region-1); simultaneously, the buffer leakage current is effectively mitigated because of the large acceptor trap density in the region-2. After the physical model and material parameter calibration [5], [7], [9], [11], [16], [23], the output and transfer characteristics of the HEMTs are validated by comparing them with measured I-V data.

IV. Results and Discussion

A. Fe-doped InAlN/GaN HEMT

Figs. 1(a) and (b) compare the measured and simulated output and transfer characteristics of Fe-doped InAlN/GaN HEMT at T_b = 303 K. The HEMT exhibits a maximum drain current of 0.735 A/mm at V_{DS} = 15 V, V_{GS} = 0 V, and a threshold voltage (V_{TH}) of -2 V. It is seen from Figs. 1(a) and (b) that the simulated I_{DS}-V_{DS} and I_{DS}-V_{GS} properties closely track the experimental I-V data.

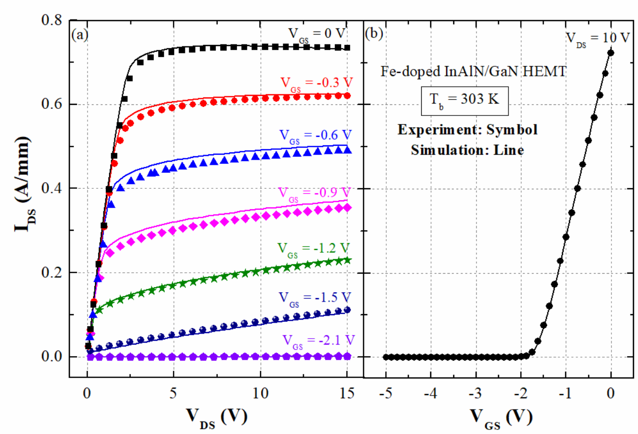

Fig. 1. Measured output (I_{DS}-V_{DS}) and transfer (I_{DS}-V_{GS}) characteristics of Fe-doped InAlN/GaN HEMT compared with the simulated I-V properties at T_b = 303 K.

The SH-induced increase in the channel temperature (ΔT) as a function of dissipated power (P_D) is plotted in Fig. 2(a). To acquire this plot, V_{DS} is varied from 1 V to 15 V for a constant V_{GS} = 0 V, and ΔT is noted for each dissipated power P_D (which is the product of I_{DS} and V_{DS} [12], [21]). The channel temperature increases linearly with the increasing power due to the lattice heating effect. The simulated lattice temperature 2D profile at the bias condition of V_{DS} = 15 V, and V_{GS} = 0 V is displayed in Fig. 2(b). As expected, the maximum electric field occurs at the drain-side of the gate-edge under a higher on-state bias voltage [12]. So, the peak channel temperature (hotspot) is detected at the gate-edge located towards the drain-side, due to the resultant high current density. Since ΔT vs. P_D plot is found to be linear in Fig. 2(a), the slope yields the thermal resistance (R_{TH} = 40.1 K/W) according to the Equation (3). This value closely matches with the result (R_{TH} = 41.7 K/W) of Oishi *et al.* [12] for the Fe-doped AlGaN/GaN HEMT on the SiC substrate. Moreover, the estimated R_{TH} is given a reasonable agreement with the R_{TH} calculated for 0.15 µm Fe-doped AlGaN/GaN HEMTs on the SiC substrate (35.25 K/W for 6×50 µm device, and 43.01 K/W for 6×75 µm device), through the two-step pulsed I-V measurements [10]. These points demonstrate the reliability of identified R_{TH} (40.1 K/W) for the Fe-doped InAlN/GaN HEMT, so this value is used to compute ΔT during the Arrhenius analysis.

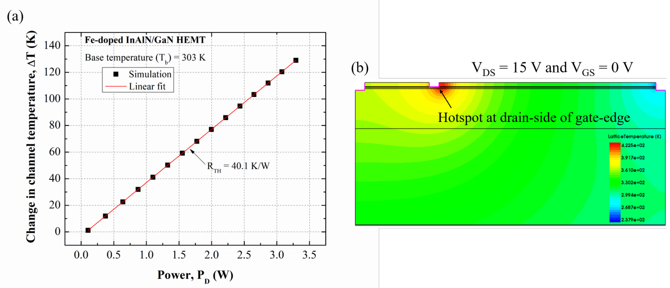

Fig. 2. (a) The SH-induced increase in the channel temperature (ΔT) as a function of dissipated power (P_D) for InAlN/GaN HEMT. (b) Simulated lattice temperature 2D profile at V_{DS} = 15 V and V_{GS} = 0 V shows the hotspot location at drain-side of the gate-edge.

Figs. 3(a) and (b) depict the DCT derivative spectra acquired with two different bias voltages (a) V_{GM} = -1.6 V, V_{DM} = 1 V and (b) V_{GM} = -1.6 V, V_{DM} = 7 V at various temperatures (303 K to 438 K). Note that, only V_{DS} is increased (fixed V_{GS} = -1.6 V) in the DCT measurements to evaluate the PF emission effect on the trap activation energy. The positive peak (F1) indicates the existence of an electron trap at E_C - E_T in the HEMT, and its emission time constant decreases with increasing temperature as per the Arrhenius law [1], [5], [8]. The DCT signal amplitude for V_{DM} = 7 V is found to be higher than its counterpart case V_{DM} = 1 V; the observed variation in the signal magnitude is due to the chosen I_{DS} range for measuring the DCT. Fig. 4(a) shows the DCT derivative spectra obtained with increasing drain voltages at T_b = 303 K (V_{DS} = 1 V to 9 V for constant V_{GS} = -1.6 V). It is observed that the emission time constant (τ_n) decreases (τ_n = 54 ms at V_{DM} = 1 V, and τ_n = 10 ms at V_{DM} = 7 V for 303 K) with the increase in the drain voltage. As the drain voltage increases in the HEMT, the accelerating electric field along the channel upsurges, so the trapped electrons require relatively lesser activation energy for thermal emission.

Fig. 4(b) depicts the Arrhenius plot for the trap F1 obtained from the DCT at V_{DM} = 1 V and 7 V bias conditions. Here ΔT correction factor is included in the Arrhenius equation to emulate the actual HEMT temperature. Subsequently, E_a and σ_n (0.6 eV, 4.5×10^{-15} cm^2 for V_{DM} = 1 V, and 0.53 eV, 6×10^{-16} cm^2 for V_{DM} = 7 V) for the trap F1 are determined from the slope and intercept of the Arrhenius plot using the Equation (4). It is found that the apparent activation energy reduces (from E_{ap} = 0.6 eV at V_{DM} = 1 V to 0.52 eV at V_{DM} = 9 V) with the increasing drain voltage, due to the PF-induced potential barrier lowering (ΔE_{PF}) effect.

Fig. 5 shows the E_{ap} vs. $(F)^{0.5}$ plot for the electron trap F1 constructed from the DCT spectroscopy. The electric field (F) at each bias condition is computed from the validated TCAD simulation results. From the simulated 2D profile, F is extracted at the point (i.e., drain-side of the gate-edge) where the electric field is maximum in the channel layer. A good linearity is obtained between E_{ap} and $(F)^{0.5}$ in Fig. 5, thus E_0 at 0.7 eV is extracted from the intercept of the plot, based on the Equation (5). This E_0 value is consistent with the result of Oishi *et al.* [12] (E_0 at 0.68 eV) and Kayis *et al.* [17] (E_0 at 0.71 eV). Moreover, Silestri *et al.* [27] experimentally identified a deep-level acceptor trap at E_C-0.7 eV in the Fe-doped AlGaN/GaN HEMT using transconductance frequency-dispersion characteristics. These literature reports [12], [17], [27] indicate the validity of the computed E_0 for the trap F1 in the InAlN/GaN HEMT. The electron trap F1 (E_0 at E_C - 0.7 eV) is attributed to the Fe-doping-related acceptor traps in the GaN buffer layer [3]-[7], [9]-[13], [22], [27].

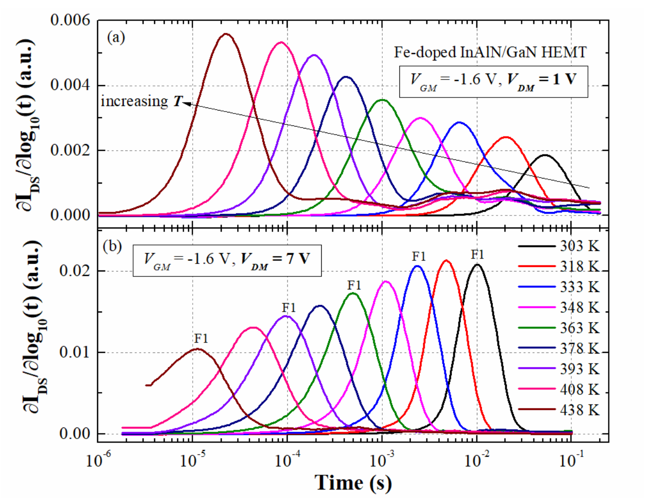

Fig. 3. DCT derivative spectra for InAlN/GaN HEMT acquired with two different bias voltages (a) V_{GM} = -1.6 V, V_{DM} = 1 V and (b) V_{GM} = -1.6 V, V_{DM} = 7 V at various temperatures (303 K to 438 K).

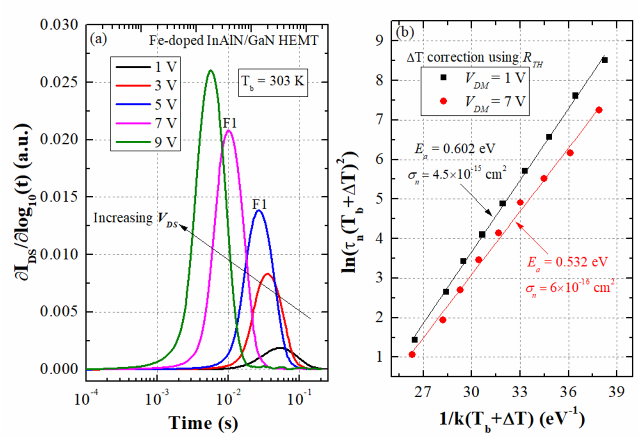

Fig. 4. (a) DCT derivative spectra measured with increasing drain voltages at T_b = 303 K (V_{DS} = 1 V to 9 V for constant V_{GS} = -1.6V). (b) Arrhenius plot (including ΔT correction) for the trap F1 obtained from the DCT at V_{DM} = 1 V and 7 V bias conditions.

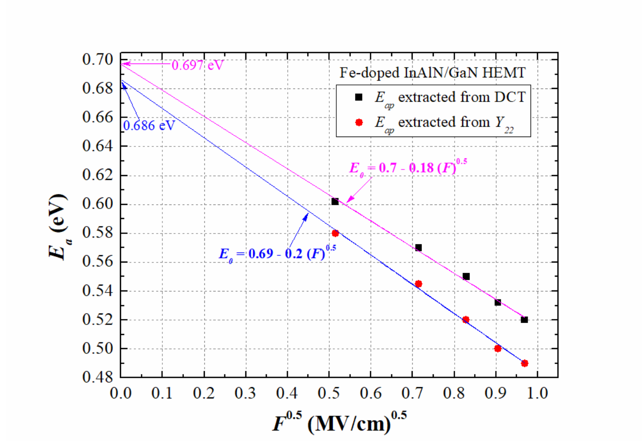

Fig. 5. E_{ap} vs. $(F)^{0.5}$ plot for the trap F1 in Fe-doped InAlN/GaN HEMT, obtained from the DCT spectroscopy and Y_{22} parameters.

Figs. 6 (a) and (b) depict the LF Y_{22} parameters measured at two different bias points (a) V_{GS} = -1.6 V, V_{DS} = 1 V and (b) V_{GS} = -1.6 V, V_{DS} = 7 V in the temperature range of 348 K to 438 K. The Y_{22} peak frequency (f_p) is related to τ_n as per the expression of $f_p = 1/2\pi\tau_n$ [8] and the peak F1 moves to the high-frequency side with the temperature rise. Due to the PF emission behavior, the emission rate speeds up with the increasing drain voltage, referring to the Y_{22} peak positions at two V_{DS} conditions in Figs. 6(a) and (b). From Y_{22} properties, E_a and σ_n for the trap F1 are computed from the Arrhenius plot for V_{DS} = 1 (0.58 eV, 7.8×10^{-15} cm^2) and V_{DS} = 7 (0.5 eV, 4.7×10^{-15} cm^2) cases. Similar to the DCT, E_{ap} decreases (from 0.58 eV at V_{DS} = 1 V to 0.49 eV at V_{DS} = 9 V) with the increase in drain voltage because of the field-assisted electron emission phenomena. Accordingly, E_{ap} vs. $(F)^{0.5}$ plot for F1 is made using the Y_{22} characteristics of the InAlN/GaN HEMT. The plot intercept provides the E_0 value of 0.69 eV for the trap F1, thereby consistent with the DCT findings (E_0 = 0.7 eV).

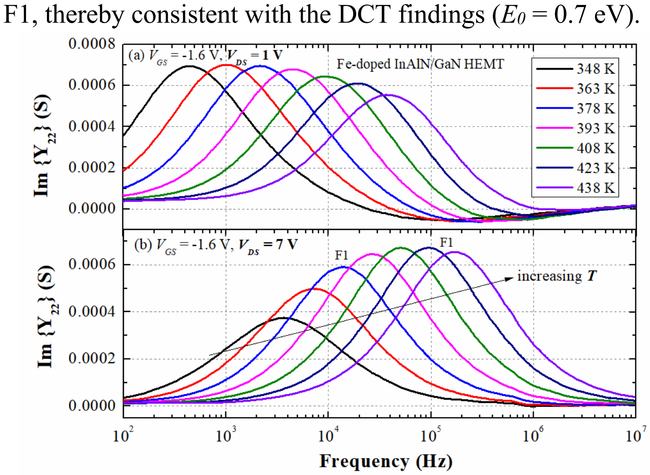

Fig. 6. LF Y_{22} parameters measured at two different bias points (a) V_{GS} = -1.6 V, V_{DS} = 1 V and (b) V_{GS} = -1.6 V, V_{DS} = 7 V in the temperature range of 348 K to 438 K.

B. C-doped AlN/GaN HEMT

Likewise, the simulated output and transfer characteristics of the C-doped AlN/GaN HEMT are validated with the measured I_{DS}-V_{DS} and I_{DS}-V_{GS} properties (not shown). The HEMT exhibits the maximum I_{DS} of 0.42 A/mm at V_{DS} = 15V, V_{GS} = 0 V and a threshold voltage of -0.8 V. The thermal resistance (R_{TH} = 35.7 K/W) is calculated from the slope of ΔT vs. P_D plot, as similar to the Fig. 2(a). The R_{TH} (35.7 K/W) value is used to calculate the ΔT based on the Equation (3), and the corrected temperature is incorporated in the Arrhenius plot analysis Equation (4).

Figs. 7(a) and (b) show the DCT derivative spectra for the C-doped AlN/GaN HEMT measured at two different bias points (a) V_{GM} = -0.3 V, V_{DM} = 1 V and (b) V_{GM} = -0.3 V, V_{DM} = 7 V at various temperatures (323 K to 403 K). A drastic reduction in the emission time constant (τ_n = 18 s at V_{DM} = 1 V and τ_n = 75 ms at V_{DM} = 1 V for T_b = 323 K) is noticed, when V_{DM} is increased from 1 V to 7 V. This reveals that the PF-emission effects are more pronounced in the C-doped AlN/GaN HEMT, as compared to the InAlN/GaN HEMT. As a result, a reduction in the E_{ap} (from 0.33 eV at V_{DM} = 1 V to 0.15 eV at V_{DM} = 9 V) is noted upon increasing the drain voltage, as determined from Arrhenius analysis Equation 4. Eventually, E_0 (at 0.51 eV) for the trap C1 is extracted from the intercept of E_{ap} vs. $(F)^{0.5}$ plot shown in Fig. 8. This E_0 value is helpful in accurately modeling the trap C1 energy position in the C-doped AlN/GaN HEMT simulations. The electron trap C1 (E_0 at E_C – 0.51 eV) may be originated from the nitrogen-vacancy and antisite (N_V and N_{Ga}) defects in the GaN buffer layer [5] or due to the extended defects observed in the C-doped GaN epilayer structure [22].

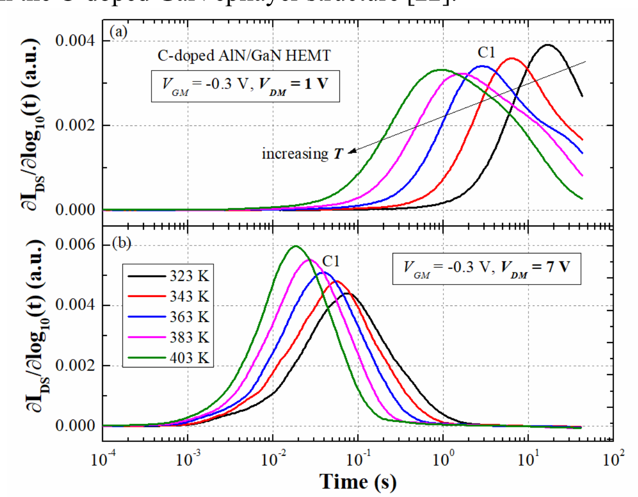

Fig. 7. DCT derivative spectra for C-doped AlN/GaN HEMT measured at two different bias points (a) V_{GM} = -0.3 V, V_{DM} = 1 V and (b) V_{GM} = -0.3 V, V_{DM} = 7 V at various temperatures (323 K to 403 K).

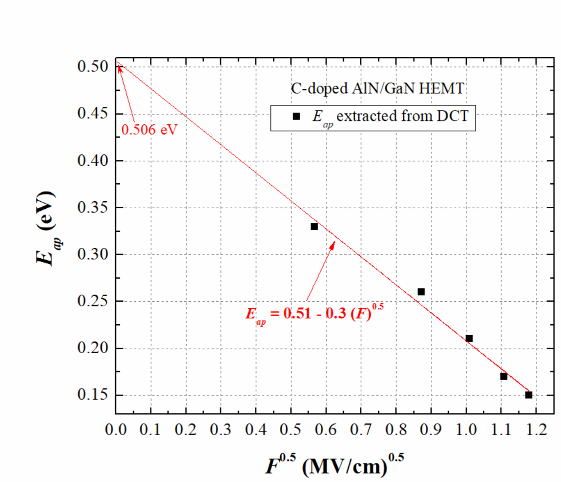

Fig. 8. E_{ap} vs. $(F)^{0.5}$ plot for the trap C1 in C-doped AlN/GaN HEMT, obtained from the DCT spectroscopy.

V. Conclusion

The zero-field activation energy (E_0) for the traps in the GaN-based HEMTs is identified by incorporating the SH and PF effects in the emission rate equation. From the validated simulation results, thermal resistance (R_{TH}) of the InAlN/GaN HEMT (40.1 K/W) and AlN/GaN HEMT (35.7 K/W) is extracted; these values are used to estimate ΔT (temperature correction) during the Arrhenius analysis. The apparent activation energy (E_{ap}) is determined from DCT/Y_{22} measurements at different V_{DS}, and the corresponding electric field (F) is computed from the simulation. Eventually, E_0 is calculated from the intercept of the E_{ap} vs. $(F)^{0.5}$ plot. E_0 at E_C -0.7 eV is found for the Fe-related buffer trap in the InAlN/GaN HEMT. E_0 for the electron trap C1 is detected at E_C – 0.51 eV in the AlN/GaN HEMT. The identified E_0 values are helpful in accurately modeling the trap activation energy in the HEMT simulations.

Acknowledgment

This work was carried out under the international research project "Trapping InvestiGation using Experimental chaRacterization and tcad Simulation (TIGERS)" between XLIM Lab, France and IIT Dharwad, India.

References

[1] D. Bisi, M. Meneghini, C. D. Santi, A. Chini, M. Dammann, P. Brückner, M. Mikulla, G. Meneghesso, and E. Zanoni, "Deep-level characterization in GaN HEMTs-part I: Advantages and limitations of drain current transient measurements," *IEEE Trans. Electron Devices,* vol. 60, no. 10, pp. 3166-3175, Oct. 2013, doi: 10.1109/TED.2013.2279021.

[2] A. Chini, F. Soci, M. Meneghini, G. Meneghesso, and E. Zanoni, "Deep levels characterization in GaN HEMTs-part II: Experimental and numerical evaluation of self-heating effects on the extraction of traps activation energy," *IEEE Trans. Electron Devices,* vol. 60, no. 10, pp. 3176-3182, Oct. 2013, doi: 10.1109/TED.2013.2278290.

[3] M. Meneghini, I. Rossetto, D. Bisi, A. Stocco, A. Chini, A. Pantellini, C. Lanzieri, A. Nanni, G. Meneghesso, and E. Zanoni, "Buffer traps in Fe-doped AlGaN/GaN HEMTs: Investigation of the physical properties based on pulsed and transient measurements," *IEEE Trans. Electron Devices*, vol. 61, no. 12, pp. 4070-4077, Dec. 2014, doi: 10.1109/TED.2014.2364855.

[4] J. Bergsten, M. Thorsell, D. Adolph, J.-T. Chen, O. Kordina, E. Ö. Sveinbjörnsson, and N. Rorsman, "Electron trapping in extended defects in microwave AlGaN/GaN HEMTs with carbon-doped buffers," *IEEE Trans. Electron Devices*, vol. 65, no. 6, pp. 2446-2453, Jun. 2018, doi: 10.1109/TED.2018.2828410.

[5] P. V. Raja, M. Bouslama, S. Sarkar, K. R. Pandurang, J.-C. Nallatamby, N. DasGupta, and A. DasGupta, "Deep-level traps in AlGaN/GaN and AlInN/GaN based HEMTs with different buffer doping technologies," *IEEE Trans. Electron Devices,* vol. 67, no. 6, pp. 2304-2310, Jun. 2020, doi: 10.1109/TED.2020.2988439.

[6] M. Cioni, N. Zagni, L. Selmi, G. Meneghesso, M. Meneghini, E. Zanoni, and A. Chini, "Electric field and self-heating effects on the emission time of iron traps in GaN HEMTs," *IEEE Trans. Electron Devices*, vol. 68, no. 7, pp. 3325-3332, Jul. 2021, doi: 10.1109/TED.2021.3081613.

[7] M. Bouslama, P. V. Raja, F. Gaillard, R. Sommet, and J.-C. Nallatamby, "Investigation of electron trapping in AlGaN/GaN HEMT with Fe-doped buffer through DCT characterization and TCAD device simulations," *AIP Adv.*, vol. 11, Dec. 2021, Art. no. 125316, doi: 10.1063/5.0064493.

[8] C. Potier, J.-C. Jacquet, C. Dua, A. Martin, M. Campovecchio, M. Oualli, O. Jardel, S. Piotrowicz, S. Laurent, R. Aubry, O. Patard, P. Gamarra, M.-A. D. Forte-Poisson, S. L. Delage, and R. Quéré, "Highlighting trapping phenomena in microwave GaN HEMTs by low-frequency S-parameters," *Int. J. Microw. Wireless Technol.*, vol. 7, nos. 3-4, pp. 287-296, Jun. 2015, doi: 10.1017/S1759078715000094.

[9] N. K. Subramani, J. Couvidat, A. A. Hajjar, J.-C. Nallatamby, R. Sommet, and R. Quéré, "Identification of GaN buffer traps in microwave power AlGaN/GaN HEMTs through low frequency S-parameters measurements and TCAD-based physical device simulations," *IEEE J. Electron Devices Soc.*, vol. 5, no. 3, pp. 175-181, May 2017, doi: 10.1109/JEDS.2017.2672685.

[10] M. Bouslama, V. Gillet, C. Chang, J.-C. Nallatamby, R. Sommet, M. Prigent, R. Quéré, and B. Lambert, "Dynamic performance and characterization of traps using different measurements techniques for the new AlGaN/GaN HEMT of 0.15-µm ultrashort gate length," *IEEE Trans. Microw. Theory Techn.*, vol. 67, no. 7, pp. 2475-2482, Jul. 2019, doi: 10.1109/TMTT.2019.2907540.

[11] P. V. Raja, N. K. Subramani, F. Gaillard, M. Bouslama, R. Sommet, and J.-C. Nallatamby, "Identification of buffer and surface traps in Fe-doped AlGaN/GaN HEMTs using Y21 frequency dispersion properties," *Electronics*, vol. 10, no. 24, Dec. 2021, Art. no. 3096, doi: 10.3390/electronics10243096.

[12] T. Oishi, T. Otsuka, M. Tabuchi, Y. Yamaguchi, S. Shinjo, and K. Yamanaka, "Bias dependence model of peak frequency of GaN trap in GaN HEMTs using low-frequency Y_{22} parameters," *IEEE Trans. Electron Devices*, vol. 68, no. 11, pp. 5565-5571, Nov. 2021, doi: 10.1109/TED.2021.3115083.

[13] T. Nishida, T. Oishi, T. Otsuka, Y.Yamaguchi, M. Tsuru, and K. Yamanaka, "Drain-bias dependence of low-frequency Y22 signals for Fe-related GaN traps in GaN HEMTs with different Fe doping concentrations," *Solid-State Electron.*, vol. 201, Mar. 2023, Art. no. 108589, doi: 10.1016/j.sse.2023.108589.

[14] O. Mitrofanov and M. Manfra, "Poole-Frenkel electron emission from the traps in AlGaN/GaN transistors," *J. Appl. Phys.*, vol. 95, no. 11, pp. 6414-6419, Jun. 2004, doi: 10.1063/1.1719264.

[15] S. Turuvekere, N. Karumuri, A. A. Rahman, A. Bhattacharya, A. DasGupta, and N. DasGupta, "Gate leakage mechanisms in AlGaN/GaN and AlInN/GaN HEMTs: Comparison and modeling," *IEEE Trans. Electron Devices*, vol. 60, no. 10, pp. 3157-3165, Oct. 2013, doi: 10.1109/TED.2013.2272700.

[16] N. K. Subramani, A. K. Sahoo, J.-C. Nallatamby, R. Sommet, N. Rolland, F. Medjdoub, and R. Quéré, "Characterization of parasitic resistances of AlN/GaN/AlGaN HEMTs through TCAD-based device simulations and on-wafer measurements," *IEEE Trans. Microw. Theory Techn.*, vol. 64, no. 5, pp. 1351-1358, May 2016, doi: 10.1109/TMTT.2016.2549528.

[17] C. Kayis, C. Y. Zhu, M. Wu, X. Li, Ü. Özgür, and H. Morkoç, "Field-assisted emission in AlGaN/GaN heterostructure field-effect transistors using low-frequency noise technique," *J. .Appl. Phys.*, vol. 109, no. 8 Apr. 2011, Art. no. 084522, doi: 10.1063/1.3576104.

[18] N. Zagni, M. Cioni, F. Iucolano, M. Moschetti, G. Verzellesi, and A. Chini, "Experimental and numerical investigation of Poole–Frenkel effect on dynamic R ON transients in C-doped p-GaN HEMTs," *Semicond. Sci. Technol.*, vol. 37, no. 2, Dec. 2021, Art. no. 025006, doi: 10.1088/1361-6641/ac4113.

[19] P. A. Martin, B. G. Streetman, and K. Hess, "Electric field enhanced emission from non-Coulombic traps in semiconductors," *J. Appl. Phys.*, vol. 52, no. 12, pp. 7409-7415, Aug. 1981, doi: 10.1063/1.328731.

[20] S. M. Sze and K. K. Ng, "Metal-insulator-semiconductor capacitors," in *Physics of Semiconductor Devices*, 3rd ed., New Jersey, USA: John Wiley & Sons, 2007, pp. 194-240.

[21] Sentaurus TCAD User Guide, Version N-2017.09, Synopsys Inc., San Jose, CA, USA, 2017.

[22] P. V. Raja, E. Dupouy, M. Bouslama, R. Sommet, and J.-C. Nallatamby, "Estimation of Trapping induced dynamic reduction in 2DEG density of GaN-Based HEMTs by gate-lag DCT technique," *IEEE Trans. Electron Devices*, vol. 69, no. 9, pp. 4864-4869, Sep. 2022, doi: 10.1109/TED.2022.3193650.

[23] P. V. Raja, J.-C. Nallatamby, N. DasGupta, and A. DasGupta, "Trapping effects on AlGaN/GaN HEMT characteristics," *Solid-State Electron.*, vol. 176, Feb. 2021, Art. no. 107929, doi: 10.1016/j.sse.2020.107929.

[24] A. Chini, V. D. Lecce, F. Soci, D. Bisi, A. Stocco, M. Meneghini, G. Meneghesso, E. Zanoni, and A. Gasparotto, "Experimental and numerical correlation between current-collapse and Fe-doping profiles in GaN HEMTs," In *IEEE International Reliability Physics Symposium (IRPS)*, Anaheim, CA, USA, Apr. 2012, pp. CD-1-4, doi: 10.1109/IRPS.2012.6241881.

[25] M. Hirose, Y. Takada, and K. Tsuda, "Numerical analysis of short-gate GaN HEMTs with Fe-doped buffer layers," *Phys. Status Solidi C*, vol. 9, no. 2, pp. 361-364, 2012, doi: 10.1002/pssc.201100283.

[26] S. Gustafsson, J.-T. Chen, J. Bergsten, U. Forsberg, M. Thorsell, E. Janzén, and N. Rorsman, "Dispersive effects in microwave AlGaN/AlN/GaN HEMTs with carbon-doped buffer," *IEEE Trans. Electron Devices*, vol. 62, no. 7, pp. 2162-2169, Jul. 2015, doi: 10.1109/TED.2015.2428613.

[27] M. Silvestri, M. J. Uren, and M. Kuball, "Iron-induced deep-level acceptor center in GaN/AlGaN high electron mobility transistors: Energy level and cross section," *Appl. Phys. Lett.*, vol. 102, no. 7, Feb. 2013, Art. no. 073501, doi: 10.1063/1.4793196.